
A Random CNN Sees Objects: One Inductive Bias of CNN and Its Applications

Yun-Hao Cao Jianxin Wu*

National Key Laboratory for Novel Software Technology
 Nanjing University, Nanjing, China
 {caoyunhao1997, wujx2001}@gmail.com

Abstract

This paper starts by revealing a surprising finding: without any learning, a randomly initialized CNN can localize objects surprisingly well. That is, a CNN has an inductive bias to naturally focus on objects, named as Tobias (“The object is at sight”) in this paper. This empirical inductive bias is further analyzed and successfully applied to self-supervised learning. A CNN is encouraged to learn representations that focus on the foreground object, by transforming every image into various versions with different backgrounds, where the foreground and background separation is guided by Tobias. Experimental results show that the proposed Tobias significantly improves downstream tasks, especially for object detection. This paper also shows that Tobias has consistent improvements on training sets of different sizes, and is more resilient to changes in image augmentations. Our codes will be available at <https://github.com/CupidJay/Tobias>.

1 Introduction

Deep convolutional neural networks (CNNs) have achieved great success in various computer vision tasks. However, as of today we still know little about what makes a CNN suitable for analyzing natural images, i.e., what is its *inductive bias*. The inductive bias of a learning algorithm specifies constraints on the hypothesis space, and a model can only be instantiated from the hypothesis space that satisfies these constraints. It is easy to reveal the inductive bias of certain learning algorithms (e.g., a linear classifier specifies a linear relationship between the features and the target variable). But, the inductive bias of complex CNNs is still hidden in the fog [6]. Successfully identifying CNN’s inductive bias will not only deepen our theoretical understanding of this complex model, but also lead to potential important algorithmic progresses.

Objects are the key in most natural images, and CNNs are good at recognizing, detecting and segmenting objects. For instance, weakly supervised object localization (WSOL) [35, 25, 33] and unsupervised object localization (USOL) methods [29, 30] can even localize objects without training on bounding box annotations. All these methods, however, *rely on ImageNet [24] pretrained models and non-trivial learning steps*.

In this paper, we first show that focusing its attention to objects is a born gift of CNNs even *without any training*, i.e., it is CNN’s inductive bias (or one inductive biases out of many) from an empirical perspective! A *randomly initialized* CNN has surprisingly good localization ability, as shown in Figure 1. We name this phenomenon “*The object is at sight*”, or “*Tobias*” for short. The object(s) miraculously pop out (“at sight”) without any need for learning. Our conjecture is: the background is relatively texture-less compared to the objects, and texture-less regions have higher chances to be deactivated by activation functions like ReLU.

*J. Wu is the corresponding author.

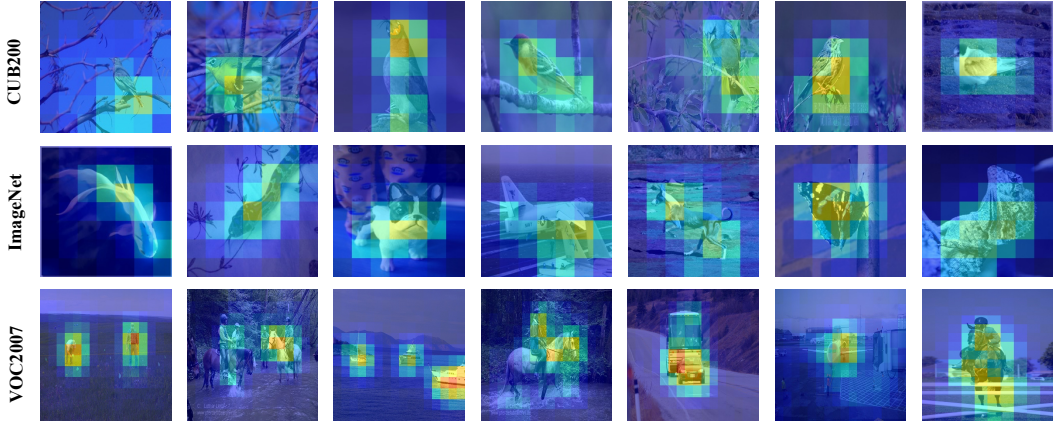


Figure 1: Visualization of localization heatmaps using SCDA [29] for a *randomly initialized* ResNet-50. Best viewed in color when zoomed in.

Tobias then lends us ‘free’ (free of labels and pretrained models) and relatively accurate supervision for where objects are. Hence, a natural application of Tobias is self-supervised learning (SSL), which aims to learn useful representations without requiring labels. After the emerging of the InfoNCE loss [27] and the contrastive learning paradigm, many SSL algorithms have been published, such as MoCo [14], SimCLR [3], BYOL [13], and many more. In this paper, we propose to probabilistically change an image’s background (selected from other images) while keep the foreground objects by using Tobias. We thus force the model to learn representations focusing on the objects.

We evaluate the representation learned by Tobias SSL on ImageNet [24] and other vision benchmarks. Our method achieves consistent improvements on various benchmarks, especially on object detection because our method can better capture the foreground objects. Also, we carefully study the influence of the number of pretraining images, and our method has consistent improvements on different amounts of training data. Our contributions are: (i) We find the “Tobias” inductive bias of CNN, i.e., a random CNN can localize objects without any learning. (ii) We successfully apply Tobias to SSL and achieve consistent improvements on various benchmarks. (iii) Our method is robust when the amount of data is small or large, and is more resilient to changes in the set of image augmentations.

2 Related Works

Random networks’ potential. [9] proposed the Lottery Ticket Hypothesis: A randomly initialized, dense neural network contains a subnetwork that is initialized such that—when trained in isolation—it can match the test accuracy of the original network after training for at most the same number of iterations. A lot of works followed this line of research [2, 11, 21]. The SSL method BYOL [13] was also motivated by the random network’s potential: the representation obtained by using fixed randomly initialized network to produce the targets can already be much better than the initial fixed representation. These works show the potential of random networks from the perspective of network pruning or self learning. We investigate it from a new perspective: a random CNN sees objects.

Un/Weakly-supervised object localization. Weakly supervised object localization (WSOL) [35, 25, 33] learns to localize objects with only image-level labels. CAM [35] generated class activation maps with the global averaging pooling (GAP) layer and the final fully connected (FC) layer (weights of the classifier). Unsupervised localization methods do not even need image-level labels. SCDA [29] aggregated information through the channel dimension to get localization masks. DDT [30] evaluated the correlation of descriptors. However, they all rely on ImageNet [24] pretrained models. Instead, our Tobias does not require any labels or pretrained models.

Self-supervised learning. Self-supervised learning (SSL) has emerged as a powerful method to learn visual representations without the expensive labels. Many recent works follow the contrastive learning paradigm [27]. SimCLR [3] and MoCo [14] trained networks to identify a pair of views originating from the same image when contrasted with a large set of views from other images. BYOL [13] discarded negative sampling by using a momentum encoder. Our method is compatible with emerging

SSL methods and only the data loader needs to be changed. The most related methods to ours are [26] and [5], where Mixup [34] or CutMix [32] was used to combine two images and force the new image to be similar to both. However, they may either generate unnatural images or cut objects out due to the lack of supervision. In contrast, our method provides free foreground vs. background supervision to merge patches, which proves to be useful in Section 4.

Data augmentation. We use Tobias to merge patches from two different images to generate a new image, which keeps the objects and replaces the background. Our method can be viewed as a data augmentation strategy. As aforementioned, Mixup [34] and CutMix [32] do not have the location information as in our method and the random cut in CutMix may cover the foreground area with the background. ‘Copy and paste’ [7, 10] is an effective augmentation in object detection and instance segmentation, which cut object instances and paste them on other images. These methods require ground-truth bounding box labels, while ours does not rely on any labels.

3 Tobias, and SSL with Tobias

Now we first introduce how a randomly initialized CNN localizes objects. Then, we introduce how Tobias is applied to self-supervised learning.

3.1 Object localization using a random CNN

Given an input image \mathbf{x} of size $H \times W$, the outputs of a CNN (before the GAP layer) are formulated as an order-3 tensor $Q \in \mathbb{R}^{h \times w \times d}$, which include a set of 2-D feature maps $S = \{S_n\} (n = 1, \dots, d)$. S_n (of size $h \times w$) is the n -th feature map of the corresponding channel (the n -th channel). For instance, by employing the ResNet-50 [17] model, Q is the output of ‘pool5’ (i.e., activations of the last max-pooling layer) and we can get a $7 \times 7 \times 2048$ tensor if the input image is 224×224 .

SCDA [29] obtains a 2-D aggregation map $A \in \mathbb{R}^{h \times w}$ by adding up Q through the depth direction and use the mean value of A as the threshold to localize objects. Formally, $A = \sum_{n=1}^d S_n$. Then, a mask map M of the same size as A can be obtained by

$$M_{i,j} = \begin{cases} 1 & \text{if } A_{i,j} > \bar{a} \\ 0 & \text{otherwise} \end{cases}, \quad (1)$$

where $\bar{a} = \frac{1}{h \times w} \sum_{i,j} A_{i,j}$ and (i, j) is a particular position in these $h \times w$ locations. Those positions (i, j) whose activation response are higher than \bar{a} (i.e., $M_{i,j} = 1$) indicate the foreground objects.

The original SCDA [29] used ImageNet pretrained models for feature extraction and localization, and obtained good localization performance. However, there are many scenarios where pretrained models do not exist. Instead, we follow the same setups as in SCDA and only replace the ImageNet pretrained weights by random weights. We find that a pretrained model is not necessary and a randomly initialized CNN can also localize objects surprisingly well. We name this phenomenon “The object is at sight”, or “Tobias” for short. Figure 1 visualizes some localization examples, and we defer more results and further analyses to Section 4.1.

3.2 Tobias self-supervised learning

Based on our finding that an un-trained random network can capture foreground objects surprisingly well (i.e., Tobias), it is natural to wonder if we can take advantage of this property in SSL, where we do not have any pretrained models or annotated labels. In this section, we propose a Tobias augmentation, which keeps the objects and probabilistically changes the background for an image, and can be integrated into any existing SSL method. Moreover, we will demonstrate that our method can be viewed as either a data augmentation or a pseudo supervised contrastive learning method.

The Tobias augmentation. We make two modifications to SCDA in order to better adapt to SSL algorithms. First, we add an extra max pooling layer (with stride=2) after ‘pool5’ and the mask map M becomes 4×4 instead of 7×7 for a 224×224 input image. The mask M for each image is pre-calculated by a randomly initialized network and do not change during further training. Second, we use *the median* instead of the mean value as the threshold to make sure that we have half the background (where $M_{i,j} = 0$) and half the foreground (where $M_{i,j} = 1$). Notice that this hard half-half division cannot fit all images exactly, because there exist images where objects cover more

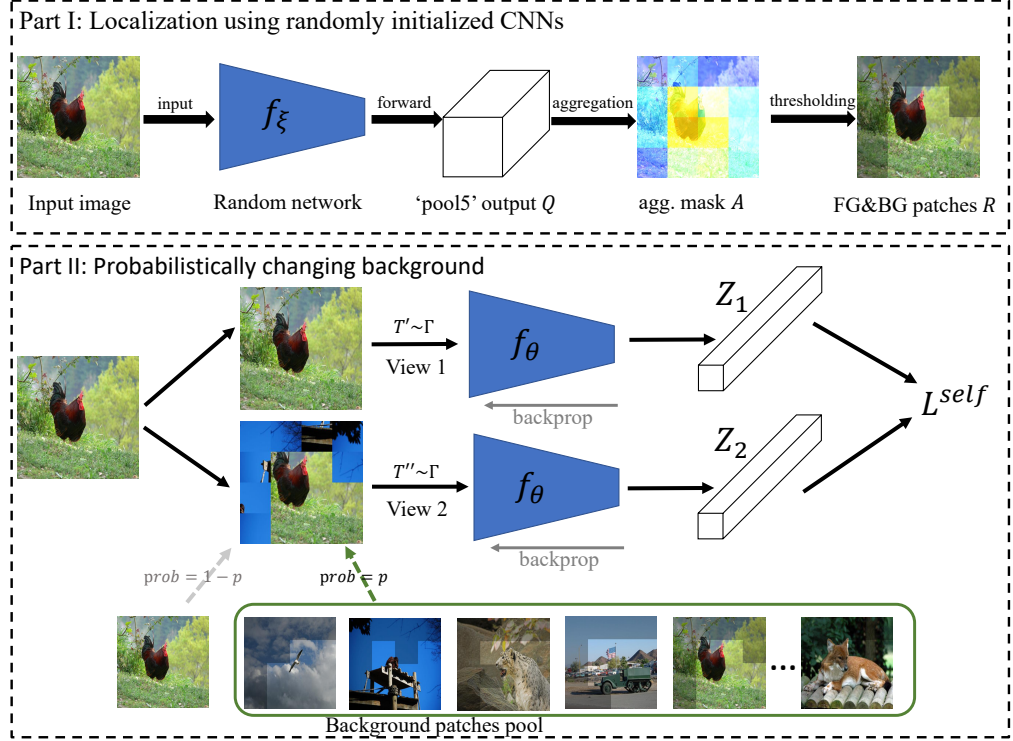


Figure 2: Pipeline of Tobias self-supervised learning. Upper part: splitting foreground and background using a *randomly initialized* CNN. Lower part: applying Tobias augmentation into SSL.

than or less than half of the area. However, this choice makes it easier when we combine foreground and background patches from two different images.

Then we split the input image \mathbf{x} into $4 \times 4 = 16$ patches $R = \{R_{i,j}\} (i, j = 0, \dots, 3)$, in which each patch corresponds to one position in M :

$$R_{i,j} = \mathbf{x}[i \times r : (i+1) \times r - 1, j \times r : (j+1) \times r - 1], \quad (2)$$

where $r \times r$ is the patch size and $r = 224/4 = 56$ in our setting, $[:, :]$ represents the slice operation. We call $R_{i,j}$ a foreground patch if $M_{i,j} = 1$ and a background patch otherwise.

Given two image \mathbf{x}_1 and \mathbf{x}_2 , we can generate a new image $\mathbf{x}_{1,2}$, which contains foreground patches in \mathbf{x}_1 and background patches in \mathbf{x}_2 . When merging patches from two images, we keep the positions of foreground patches unchanged and fill in other positions with background patches in a random order. Let $R^{(1)}$, $R^{(2)}$ and $R^{(1,2)}$ denote the patches in \mathbf{x}_1 , \mathbf{x}_2 and $\mathbf{x}_{1,2}$, respectively. Then,

$$R_{i,j}^{(1,2)} = \begin{cases} R_{i,j}^{(1)} & \text{if } M_{i,j}^{(1)} = 1 \\ R_{\sigma(i,j)}^{(2)} & \text{otherwise} \end{cases}, \quad (3)$$

where $\sigma(\cdot, \cdot)$ defines a one-to-one mapping from background positions in \mathbf{x}_1 to background positions in \mathbf{x}_2 . More specifically, background positions in \mathbf{x} means $\{(i, j) | M_{i,j} = 0\}$ and σ defines such a random order to fill in background patches. Notice that all images have the same number of foreground and background patches and we are safe and free to merge these patches.

Applying Tobias to SSL. We now apply Tobias to the contrastive learning paradigm following the notations in SupCon [18]. Suppose the dataset D has a total of N_t images and we randomly sample N images $\{\mathbf{x}_k\}_{k=1 \dots N}$ to form a batch. The corresponding batch used for training consists of $2N$ pairs, $\{\mathbf{x}'_k, \mathbf{x}''_k\}_{k=1 \dots N}$, where \mathbf{x}'_k and \mathbf{x}''_k are two random augmentations (i.e., “views”) of \mathbf{x}_k . We denote the transformation as T , which is sampled from the predefined augmentation function space Γ . Hence we have $\mathbf{x}'_k = T'(\mathbf{x}_k)$ and $\mathbf{x}''_k = T''(\mathbf{x}_k)$, where $T', T'' \sim \Gamma$. In self-supervised contrastive

learning (e.g., SimCLR [3], MoCo [14]), the loss takes the following form:

$$L^{self} = - \sum_i \log \frac{\exp(\mathbf{z}'_i \cdot \mathbf{z}''_i)/\tau}{\sum_{j \neq i} \exp(\mathbf{z}'_i \cdot \mathbf{z}'_j/\tau) + \sum_j \exp(\mathbf{z}'_i \cdot \mathbf{z}''_j/\tau)}, \quad (4)$$

where $\mathbf{z}'_i = f(\mathbf{x}'_i)$, $\mathbf{z}''_i = f(\mathbf{x}''_i)$, the \cdot symbol denotes the inner product and τ is the temperature parameter. Here $f(\cdot) \equiv \text{Proj}(\text{Enc}(\cdot))$ denotes the composition of encoder and projection networks.

Then we introduce Tobias into SSL. Given an image \mathbf{x}_k , we generate the first view as before, i.e., $\mathbf{x}'_k = T'(\mathbf{x}_k)$. However, for another view \mathbf{x}''_k , we transform \mathbf{x}_k into $\mathbf{x}_{k,m}$ by changing its background patches with another randomly selected image \mathbf{x}_m with probability p , where p is a hyper-parameter:

$$\begin{cases} Pr(\mathbf{x}''_k = T''(\mathbf{x}_k)) = 1 - p \\ Pr(\mathbf{x}''_k = T''(\mathbf{x}_{k,m})) = \frac{p}{N_t} \end{cases}, m = 1, \dots, N_t \quad . \quad (5)$$

Hence, the loss function becomes

$$L^{Tobias} = - \sum_i \log \frac{\exp(\mathbf{z}'_i \cdot \mathbf{z}^p_i)/\tau}{\sum_{j \neq i} \exp(\mathbf{z}'_i \cdot \mathbf{z}'_j/\tau) + \sum_j \exp(\mathbf{z}'_i \cdot \mathbf{z}^p_j/\tau)}, \quad (6)$$

where $\mathbf{z}^p_i = f(\mathbf{x}^p_i)$ and \mathbf{x}^p_i is one of the augmented samples in $P(i) \equiv \{\mathbf{x}_i, \mathbf{x}_{i,1}, \dots, \mathbf{x}_{i,N_t}\}$, which follows the distribution in Equation 5. Notice that when $p = 0$, L^{Tobias} degenerates into L^{self} . Furthermore, Equation 6 can be seen as a pseudo supervised contrastive loss, where $P(i)$ contains images with the same foreground object.

4 Experimental Results

We use CUB-200 [28] and ImageNet [24] for our experiments. First, we show the localization results of randomly initialized CNNs and make further analyses in Section 4.1. Then, we apply our Tobias method into SSL and demonstrate its effectiveness across various pretraining datasets, downstream tasks, backbone architectures and SSL algorithms in Section 4.2. Finally, we study the effects of different components and hyper-parameters and sensitivity to data augmentations in our algorithm in Section 4.3. All our experiments were conducted using PyTorch [22] and we used 8 Titan Xp GPUs for our experiments. Codes will be made publicly available soon.

4.1 Localization ability of random CNNs

In this section, we study the localization ability of randomly initialized CNNs. We use SCDA [29] for localization and conduct experiments on two popular datasets for object localization, i.e., ImageNet [24] and CUB-200 [28]. Notice that [29] used ImageNet pretrained models for evaluation while we study the potential of randomly initialized models here. The localization is correct when the intersection over union (IoU) between the ground truth bounding box and the predicted box is 50% or more. In Table 1, we report the average localization accuracy and standard deviation of 3 trials for randomly initialized models and we adopt Kaiming initialization [16] used in the PyTorch official code. We use the PyTorch official models for ImageNet pretrained models. We show some visualization results on CUB-200, ImageNet as well as one complex multi-object dataset Pascal VOC2007 [8] in Figure 1. The heatmap in Figure 1 is calculated by the 2-D aggregation mask A , as noted in Section 3.1. More visualization results for Table 1 and discussions about the effect of other random initialization methods (e.g., Xavier initialization [12]) are included in the appendix.

As shown in Table 1, randomly initialized ResNet-18 and ResNet-50 [17] achieve comparable localization accuracies with their ImageNet supervised counterparts on both ImageNet and CUB-200. We also present one popular WSOL method CAM [35] for comparison and it further shows that our results for random CNNs are accurate. Notice that SCDA relies only on convolution feature maps while CAM also relies on the trained FC weights, hence we can see a significant drop for CAM with randomly initialized models. Also, from Figure 1 we can observe more intuitively that randomly initialized CNNs can not only locate a single object, but multiple objects as well. Furthermore, we can observe that the standard deviation of multiple trials is small for randomly initialized models (also see the appendix—there is only small difference between the visualization results of different trials). The results show that a randomly initialized CNN can achieve surprisingly good localization results and the localization results are robust with different random weights.

Table 1: Comparisons of localization accuracy between ImageNet pretrained and randomly initialized CNNs on ImageNet and CUB-200. ‘R18’ and ‘R50’ are the abbreviations for ResNet-18 and ResNet-50, respectively. ‘#ReLU’ and ‘#MP’ represents the number of ReLU units and max pooling layers, respectively. ‘IN super.’ stands for ‘ImageNet supervised’. We report the average accuracy and standard deviation of 3 trials for randomly initialized models.

Method	Backbone	#ReLU/#MP	ImageNet		CUB-200	
			IN super.	random init.	IN super.	random init.
SCDA [29]	R18	9 / 5	53.5	48.5±0.6	44.2	39.0±0.4
	R50	33 / 5	51.9	48.2±0.6	44.8	41.8±0.6
	R50 (sigmoid)	0 / 5	46.9	45.5±1.9	32.6	22.6±3.3
	R50 (arctan)	0 / 5	34.4	36.6±0.7	19.1	18.1±0.3
	R50 (conv1)	1 / 1	44.1	41.3±1.5	33.8	30.5±1.0
	R50 (conv1-2)	7 / 2	38.4	39.7±1.5	22.1	29.6±0.9
	R50 (conv1-3)	15 / 3	45.0	42.2±0.9	31.0	31.8±0.2
	R50 (conv1-4)	27 / 4	49.9	47.2±1.3	39.2	40.1±0.4
CAM [35]	R50	33 / 5	52.9	33.8±0.1	50.0	26.0±0.3

But, why can a random CNN see objects without any learning? Given the empirical results and in particular its stability under different random initializations, we believe it is the inductive bias of modern CNNs. There are a lot of ReLU and max pooling layers inside ResNet-50 (and most other modern CNNs). Remember that SCDA simply adds feature maps across the channel dimension. Hence, if one spatial location has many zeros (i.e., deactivated after ReLU), we expect it to have a low SCDA score and thus being predicted as belonging to the background.

Our conjecture is then: *the background is relatively texture-less when compared to the objects, and texture-less regions have higher chances to be deactivated by ReLU and max pooling*. We design two experiments to verify it. One is to replace all ReLU activations with other activation functions (e.g., sigmoid). The other one is to gradually reduce the number of ReLU units and we directly remove whole stages for ResNet-50. For instance, ‘conv1-4’ means that we remove the last stage in ResNet-50 (i.e., ‘conv5’). From Table 1 we can have the following two conclusions. First, ReLU plays an important role because when we replace ReLU with sigmoid or arctan, a significant decrease in localization accuracy was observed (c.f. appendix for visualization). Second, max pooling is also important. If we compare ‘R18’ with ‘R50 (conv1-3)’, the former has fewer convolutions and ReLUs but more max pooling, and its accuracy is higher. Visualization in the appendix more intuitively shows that shallow layers (e.g., ‘conv1’ or ‘conv1-2’) are confused by edges in backgrounds (such as grass or floor) but the full network can successfully see the whole object.

In short, we find that randomly initialized CNNs can localize objects surprisingly well, which is even comparable to their supervised counterparts. Also, we analyze the effect of different components in modern ResNets. The results reveal the potential of a random CNN in localizing objects and provide a new perspective to explain why modern CNNs achieve such good performance in visual analysis.

4.2 Tobias self-supervised learning

Now we apply Tobias to SSL (Equation 6) and evaluate its effectiveness on CUB200 in Section 4.2.1 and ImageNet in Section 4.2.2. We will analyze the effects of different components and hyper-parameters and sensitivity to data augmentations in Section 4.3.

4.2.1 Results on CUB-200

We carefully study our Tobias using 2 typical SSL methods, namely MoCov2 [4] and SimCLR [3] under both ResNet-18 and ResNet-50 [17]. We follow the training and evaluation protocols in [1] and conduct experiments on CUB-200 [28]. The full learning process contains two stages: pretraining and fine-tuning. We use the pretrained weights obtained by SSL for initialization and then fine-tune networks for classification using the cross entropy loss. Note that *SSL pretraining and fine-tuning are both performed only on the target dataset CUB-200* in this subsection.

For the fine-tuning stage, we fine-tune all methods for 120 epochs using SGD with a batch size of 64, a momentum of 0.9 and a weight decay of 5e-4 for fair comparison. The learning rate starts from 0.1 with cosine learning rate decay. We also list the results using the Mixup [34] strategy, where the alpha

Table 2: Comparisons of pretraining details and accuracies (%) on CUB-200. ‘N/A’ means that pretraining are conducted on ImageNet instead of CUB-200 for ImageNet supervised models.

Backbone	SSL pretraining		Fine-tuning accuracy (%)	
	method	epochs	Normal fine-tune	Mixup fine-tune
ResNet-18	ImageNet super.	N/A	76.2	75.0
	random init.	0	62.0	63.4
	MoCov2	200	63.7	65.8
	MoCov2-Tobias		64.4 (+0.7)	66.3 (+0.5)
	MoCov2	800	65.0	66.3
	MoCov2-Tobias		66.2 (+1.2)	67.7 (+1.4)
	SimCLR	200	63.6	64.5
	SimCLR-Tobias		65.4 (+1.8)	68.6 (+4.1)
ResNet-50	SimCLR	800	66.0	67.3
	SimCLR-Tobias		67.4 (+1.4)	69.3 (+2.0)
	ImageNet super.	N/A	81.3	82.1
	random init.	0	58.6	56.3
	MoCov2	200	56.2	53.0
	MoCov2-Tobias		63.6 (+7.4)	62.0 (+9.0)
	MoCov2	800	66.5	62.0
	MoCov2-Tobias		67.2 (+0.7)	71.5 (+9.5)
	SimCLR	200	68.0	66.5
	SimCLR-Tobias		68.4 (+0.4)	71.7 (+5.2)
	SimCLR	800	69.2	73.0
	SimCLR-Tobias		70.0 (+0.8)	73.6 (+0.6)

Table 3: Left: Object detection and instance segmentation on COCO (bounding-box AP (AP^{bb}) and mask AP (AP^{mk}) evaluated on val2017); Right: Object detection on PASCAL VOC trainval07+12 (default VOC metric AP_{50} , COCO-style AP, and AP_{75} evaluated on test2007).

pretraining method	R50-FPN (1x)						R50-FPN (24k)			R-50 C4 (24k)		
	AP^{bb}	AP_{50}^{bb}	AP_{75}^{bb}	AP^{mk}	AP_{50}^{mk}	AP_{75}^{mk}	AP_{50}	AP	AP_{75}	AP_{50}	AP	AP_{75}
random init.	31.0	49.5	33.2	28.5	46.8	30.4	63.0	36.7	36.9	60.2	33.8	33.1
IN supervised	38.4	59.2	41.6	35.0	55.9	37.1	80.8	53.5	58.4	81.3	53.5	58.8
MoCov2 200ep	39.0	59.5	42.4	35.6	56.6	38.0	81.8	55.0	60.5	82.2	57.1	64.5
MoCov2-Tobias 200ep	39.3	59.9	42.7	35.8	56.9	38.4	82.0	55.5	61.1	82.6	57.7	64.9
MoCov2 800ep	39.5	59.8	43.2	36.0	56.9	38.6	81.5	55.0	61.0	82.6	57.7	64.5

(a) COCO2017

(b) Pascal VOC 07&12

is set to 1.0. For the SSL pretraining stage, we follow the same settings in the original papers and more details are included in the appendix. ‘-Tobias’ denotes our method and we only change the data loading process and other training settings remain the same as baseline methods for fair comparison.

The results are shown in Table 2. Tobias has consistent improvements under various backbones, pretraining epochs and SSL algorithms. Taking ResNet-50 as an example, our Tobias achieves 13.2% relative higher accuracies than the baseline MoCov2 with normal fine-tuning when both pretrained for 200 epochs. Also, the relative improvement has risen to 17.0% if we use mixup. It indicates that our method is more friendly to subsequent fine-tuning with mixup because our model has learned better foreground invariance during pretraining. From this perspective, our Tobias can be seen as an informative Mixup or CutMix [32] (with foreground vs. background information). We will further demonstrate the effectiveness of such foreground vs. background information in Section 4.3.

4.2.2 Results on ImageNet

Now we move on to the large-scale dataset ImageNet [24]. We use MoCov2 for illustration following the official training and evaluation protocols in [4]. We adopt ResNet-50 as backbone and set the batch size to 256, learning rate to 0.03, number of epochs to 200 and memory bank size to 65536 as in [4]. We carefully investigate the downstream object detection performance on COCO2017 [20] and Pascal VOC 07&12 in Table 3. The detector is Faster R-CNN [23] with a backbone of R50-FPN [19] or R50-C4 [15] for Pascal VOC, and Mask R-CNN [15] with R50-FPN backbone for COCO, implemented in [31]. Also, we experimented on 8 downstream classification benchmarks following [1] in Table 4 and more details are included in the appendix.

Table 4: Transfer learning results from ImageNet with standard ResNet-50 architecture.

Method	ImageNet	VOC2007	CUB200	Cars	Aircrafts	Caltech-101	Flowers	Dogs	DTD
<i>Linear evaluation:</i>									
MoCov2 200ep	67.7	80.6	17.8	14.1	12.3	80.8	68.5	42.1	64.9
MoCov2-Tobias 200ep	67.4	82.0	18.2	12.3	12.9	81.7	70.1	42.9	63.9
IN supervised	-	73.9	61.7	47.1	23.7	89.1	86.9	82.2	68.2
<i>Fine-tuned:</i>									
MoCov2 200ep	73.9	85.6	75.5	89.2	86.5	89.2	95.7	76.6	68.6
MoCov2-Tobias 200ep	74.0	86.3	76.1	89.5	87.8	90.7	96.2	77.5	68.2
IN supervised	76.1	89.0	81.3	90.6	86.7	94.1	96.7	80.1	74.7

Table 5: Downstream object detection performance on VOC 07&12 and linear evaluation accuracy on Tiny-ImageNet-200 when pretrained on ImageNet subsets using ResNet-50.

pretraining			VOC 07&12			Tiny-IN-200
method	#images	epochs	AP ₅₀	AP	AP ₇₅	
random init.	0	0	63.0	36.7	36.9	0.5
MoCov2	10,000	200	71.1	43.6	45.8	0.5
MoCov2-Tobias			71.4 (+0.3)	44.3 (+0.7)	47.0 (+1.2)	9.9 (+9.4)
MoCov2	10,000	800	71.6	43.9	45.9	23.6
MoCov2-Tobias			73.2 (+1.6)	45.7 (+1.8)	48.5 (+2.6)	23.9 (+0.3)
MoCov2-RM			72.0 ↓1.2	44.5 ↓1.2	47.4 ↓1.1	23.5 ↓0.4
MoCov2	50,000	200	72.2	44.7	46.8	26.3
MoCov2-Tobias			73.7 (+1.5)	46.0 (+1.3)	49.2 (+2.4)	26.0 (-0.3)
MoCov2	50,000	800	77.5	49.3	53.3	37.9
MoCov2-Tobias			77.9 (+0.4)	50.3 (+1.0)	54.9 (+1.6)	40.7 (+2.8)
MoCov2-RM			77.4 ↓0.5	49.7 ↓0.6	53.3 ↓1.6	40.1 ↓0.6
MoCov2	100,000	200	76.2	48.0	51.6	35.3
MoCov2-Tobias			77.5 (+1.3)	49.8 (+1.8)	53.9 (+2.3)	36.5 (+1.2)
MoCov2	100,000	800	78.7	51.5	56.3	43.7
MoCov2-Tobias			79.4 (+0.7)	52.3 (+0.8)	57.3 (+1.0)	44.3 (+0.6)

As shown in Table 3, Tobias achieves better performance than baseline MoCov2 on both COCO and Pascal VOC. Also notice that our Tobias even achieves slightly better performance than MoCov2 800ep (pretrained much longer) on Pascal VOC. Also, Table 4 shows that although our Tobias achieves slightly lower accuracy in ImageNet linear evaluation, it outperforms MoCov2 baseline on 6 out of 8 downstream classification benchmarks in linear evaluation and 7 out of 8 in fine-tuning.

Apart from the full large-scale ImageNet dataset, we also study the performance under different data volumes by sampling the original ImageNet to smaller subsets, motivated by [1]. We randomly sample (*without using any image label*) 10 thousand (10k), 50 thousand (50k) and 100 thousand (100k) images to construct IN-10k, IN-50k and IN-100k, respectively. We only change the amount of data here and other training settings remain the same as before. The results are shown in Table 5 and we adopt Pascal VOC 07&12 for object detection and Tiny-ImageNet-200 (100,000 training and 10,000 validation images from 200 classes at 64x64 resolution) for linear evaluation.

As can be seen in Table 5 and Figure 3, our Tobias achieves significant improvements on both downstream tasks, especially on VOC 07&12 object detection. For instance, when both trained for 200 epochs on IN-100k (100,000 images), our Tobias is significantly better than baseline counterpart: up to **+1.3** AP₅₀, **+1.8** AP and **+2.3** AP₇₅. Also notice that when both trained for 200 epochs on IN-10k (10,000 images), MoCov2 performs the same as random guess (0.5%) while our method learns much better representations (9.9%) in terms of Tiny-IN-200 linear evaluation. In general, our method improves the most on AP₇₅, which is a more stringent metric for detection accuracy. It indicates that our model can better capture foreground objects across changing backgrounds during pretraining, hence improving performance for object detection as well as image classification. Moreover, our method is especially effective (i.e., has greater improvements) when the amount of data is small.

4.3 Ablation studies

In this section, we will first study the effectiveness of the foreground vs. background (Tobias) information (generated by random networks). Then, we will study the effect of the hyper-parameter p in our method. Finally, we study the sensitivity to data augmentations.

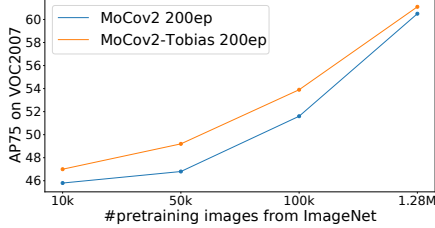


Figure 3: Performance of Tobias on Pascal VOC (AP₇₅) with respect to different training data size, compared to the MoCov2 baseline.

Table 6: Effect of hyper-parameter p . All settings are pretrained on IN-10k for 800 epochs using ResNet-50.

prob p	VOC 07&12			Tiny-IN-200
	AP ₅₀	AP	AP ₇₅	
0.0	71.6	43.9	45.9	23.6
0.3	73.2	45.7	48.5	23.9
0.5	73.9	46.3	49.4	23.3
0.7	72.3	44.8	47.4	25.4
1.0	71.8	44.3	46.6	24.3

Table 7: Impact of progressively removing transformations. All pretrained on IN-10k for 800 epochs.

transformation set	MoCov2				MoCov2-Tobias			
	AP ₅₀	AP	AP ₇₅	Tiny-IN	AP ₅₀	AP	AP ₇₅	Tiny-IN
baseline	71.6	43.9	45.9	23.6	73.2	45.7	48.5	23.9
remove grayscale	70.2	42.4	44.1	19.9 _{↓ 3.7}	73.1	46.0	49.0	22.7 _{↓ 1.2}
remove color	71.3	43.8	46.0	18.1 _{↓ 5.5}	72.7	45.4	48.2	21.2 _{↓ 2.7}
crop+flip only	71.0	44.0	46.2	16.8 _{↓ 6.8}	72.9	45.6	48.3	20.2 _{↓ 3.7}
crop only	71.7	44.0	46.7	15.0 _{↓ 8.6}	73.1	46.4	49.9	17.9 _{↓ 6.0}

Effect of Tobias information. Notice that we use the foreground vs. background information when merging patches from two images. To demonstrate its effectiveness, we design a random merging strategy for comparison (MoCov2-RM in Table 5). More specifically, we do not use such information and randomly select patches from two images for merging (also half-half division) and it can also be viewed as one kind of patch-level CutMix [32, 26]. We keep all other settings the same and conduct pretraining on both IN-10k and IN-50k. As can be seen in Table 5, we will see a significant drop, especially in object detection performance if we discard the foreground vs. background information provided by our Tobias: up to **-1.2** AP₅₀, **-1.2** AP and **-1.1** AP₇₅ when trained on IN-10k for 800 epochs. It demonstrates the Tobias information provided by a randomly initialized network is vital. Another interesting thing is that RM achieves better performance than the baseline MoCov2, which indicates that this kind of data augmentation is somehow useful for SSL, as shown in [26, 5].

Effect of hyper-parameter. Now we study the effect of the hyper-parameter p , i.e., the probability of changing backgrounds in another view. We study $p = 0, 0.3, 0.5, 0.7$ and 1.0 . Notice that when $p=0$, our Tobias degenerates into the baseline MoCov2. We train on IN-10k for 800 epochs for all settings and the results are shown in Table 6. For object detection, we can observe that when p grows, the result becomes better and will not continue to improve when it grows beyond 0.5. For Tiny ImageNet linear evaluation, $p = 0.7$ achieves the highest accuracy. Notice that we directly set p to 0.3 for all our experiments throughout this paper and did not tune it under different settings. It also indicates that we can get better results with more carefully tuned hyper-parameter p (see appendix). We further study the influence of data volume on hyper-parameter selection in the appendix.

Sensitivity to image augmentations. Now we study the sensitivity to image augmentations of our Tobias by progressively removing transformations in the transformation set following [13]. The results in Table 7 show that the performance of Tobias is much less affected than the performance of MoCov2 when removing the color distortion from the set of image augmentations, especially on Tiny-IN-200. Also we can observe that color distortion (e.g., grayscale and color-jitter) has greater impact on downstream image classification and less impact on object detection. When image augmentations are reduced to a mere random crop, the gap between our Tobias and baseline MoCov2 has increased to 2.9 and 3.2 points for Tiny-IN-200 and VOC detection (AP₇₅), respectively. It indicates that our Tobias is itself an effective data augmentation and less sensitive to other augmentations.

5 Conclusions

In this paper, we revealed and analyzed the phenomenon that a randomly initialized CNN has the potential to localize objects well, which we named Tobias. Then, we proposed Tobias self-supervised learning, which forces the model to focus on foreground objects by dynamically changing backgrounds while keeping the objects under the guidance of Tobias. Various experiments have

shown that our method obtained a significant edge over baseline counterparts because it learns to better capture foreground objects. In the future, we will try to apply our Tobias to supervised learning and further explore the potential of random networks.

References

- [1] Yun-Hao Cao and Jianxin Wu. Rethinking self-supervised learning: Small is beautiful. *arXiv preprint arXiv:2103.13559*, 2021.
- [2] Tianlong Chen, Jonathan Frankle, Shiyu Chang, Sijia Liu, Yang Zhang, Michael Carbin, and Zhangyang Wang. The lottery tickets hypothesis for supervised and self-supervised pre-training in computer vision models. In *The IEEE Conference on Computer Vision and Pattern Recognition*, page in press, 2021.
- [3] Ting Chen, Simon Kornblith, Mohammad Norouzi, and Geoffrey Hinton. A simple framework for contrastive learning of visual representations. In *The International Conference on Machine Learning*, pages 1597–1607, 2020.
- [4] Xinlei Chen, Haoqi Fan, Ross Girshick, and Kaiming He. Improved baselines with momentum contrastive learning. *arXiv preprint arXiv:2003.04297*, 2020.
- [5] Xiangxiang Chu, Xiaohang Zhan, and Xiaolin Wei. Beyond single instance multi-view unsupervised representation learning. *arXiv preprint arXiv:2011.13356*, 2020.
- [6] Nadav Cohen and Amnon Shashua. Inductive bias of deep convolutional networks through pooling geometry. In *The International Conference on Learning Representations*, pages 1–28, 2017.
- [7] Debidatta Dwibedi, Ishan Misra, and Martial Hebert. Cut, paste and learn: Surprisingly easy synthesis for instance detection. In *The IEEE International Conference on Computer Vision*, pages 1301–1310, 2019.
- [8] Mark Everingham, Luc Van Gool, Christopher KI Williams, John Winn, and Andrew Zisserman. The PASCAL visual object classes (VOC) challenge. *International Journal of Computer Vision*, 88(2):303–338, 2010.
- [9] Jonathan Frankle and Michael Carbin. The lottery ticket hypothesis: Finding sparse, trainable neural networks. In *The International Conference on Learning Representations*, pages 1–13, 2019.
- [10] Golnaz Ghiasi, Yin Cui, Aravind Srinivas, Rui Qian, Tsung-Yi Lin, Ekin D.Cubuk, Quoc V. Le, and Barret Zoph. Simple copy-paste is a strong data augmentation method for instance segmentation. *arXiv preprint arXiv:2012.07177v1*, 2012.
- [11] Sharath Girish, Shishira R. Maiya, Kamal Gupta, Hao Chen, Larry Davis, and Abhinav Shrivastava. The lottery ticket hypothesis for object recognition. In *The IEEE Conference on Computer Vision and Pattern Recognition*, page in press, 2021.
- [12] Xavier Glorot and Yoshua Bengio. Understanding the difficulty of training deep feedforward neural networks. In *Proceedings of the Thirteenth International Conference on Artificial Intelligence and Statistics*, volume 9, pages 249–256, 2010.
- [13] Jean-Bastien Grill, Florian Strub, Florent Altche, Corentin Tallec, Pierre H.Richemond, Elena Buchatskaya, Carl Doersch, Bernardo Avila Pires, Zhaohan Daniel Guo, Mohammad Gheshlaghi Azar, Bial Piot, Koray Kavukcuoglu, Remi Munos, and Michal Valko. Boostrap your own latent: A new approach to self-supervised learning. In *Advances in Neural Information Processing Systems*, pages 21271–21284, 2020.
- [14] Kaiming He, Haoqi Fan, Yuxin Wu, Saining Xie, and Ross Girshick. Momentum contrast for unsupervised visual representation learning. In *The IEEE Conference on Computer Vision and Pattern Recognition*, pages 9729–9738, 2020.
- [15] Kaiming He, Georgia Gkioxari, Piotr Dollár, and Ross Girshick. Mask R-CNN. In *The IEEE International Conference on Computer Vision*, pages 2961–2969, 2017.
- [16] Kaiming He, Xiangyu Zhang, Shaoqing Ren, and Jian Sun. Delving deep into rectifiers: Surpassing human-level performance on imagenet classification. In *The IEEE International Conference on Computer Vision*, pages 1026–1034, 2015.

- [17] Kaiming He, Xiangyu Zhang, Shaoqing Ren, and Jian Sun. Deep residual learning for image recognition. In *The IEEE Conference on Computer Vision and Pattern Recognition*, pages 770–778, 2016.
- [18] Prannay Khosla, Piotr Teterwak, Chen Wang, Aaron Sarna, Yonglong Tian, Phillip Isola, Aaron Maschinot, Ce Liu, and Dilip Krishnan. Supervised contrastive learning. In *Advances in Neural Information Processing Systems*, pages 18661–18673, 2020.
- [19] Tsung-Yi Lin, Piotr Dollár, Ross Girshick, Kaiming He, Bharath Hariharan, and Serge Belongie. Feature pyramid networks for object detection. In *The IEEE Conference on Computer Vision and Pattern Recognition*, pages 2177–2125, 2017.
- [20] Tsung-Yi Lin, Michael Maire, Serge Belongie, James Hays, Pietro Perona, Deva Ramanan, Piotr Dollár, and C Lawrence Zitnick. Microsoft COCO: Common objects in context. In *The European Conference on Computer Vision*, volume 8693 of *LNCS*, pages 740–755. Springer, 2014.
- [21] Eran Malach, Gilad Yehudai, Shai Shalev-Schwartz, and Ohad Shamir. Proving the lottery ticket hypothesis: Pruning is all you need. In *The International Conference on Machine Learning*, pages 6682–6691, 2020.
- [22] Adam Paszke, Sam Gross, Francisco Massa, Adam Lerer, James Bradbury, Gregory Chanan, Trevor Killeen, Zeming Lin, Natalia Gimelshein, Luca Antiga, Alban Desmaison, Andreas Kopf, Edward Yang, Zachary DeVito, Martin Raison, Alykhan Tejani, Sasank Chilamkurthy, Benoit Steiner, Lu Fang, Junjie Bai, and Soumith Chintala. Pytorch: An imperative style, high-performance deep learning library. In *Advances in Neural Information Processing Systems*, pages 8024–8035, 2019.
- [23] Shaoqing Ren, Kaiming He, Ross Girshick, and Jian Sun. Faster R-CNN: Towards real-time object detection with region proposal networks. In *Advances in Neural Information Processing Systems*, pages 91–99, 2015.
- [24] Olga Russakovsky, Jia Deng, Hao Su, Jonathan Krause, Sanjeev Satheesh, Sean Ma, Zhiheng Huang, Andrej Karpathy, Aditya Khosla, Michael Bernstein, Alexander C. Berg, and Li Fei-Fei. ImageNet large scale visual recognition challenge. *International Journal of Computer Vision*, 115(3):211–252, 2015.
- [25] Ramprasaath R. Selvaraju, Michael Cogswell, Abhishek Das, Ramakrishna Vedantam, Devi Parikh, and Dhruv Batra. Grad-CAM: Visual explanations from deep networks via gradient-based localization. In *The IEEE International Conference on Computer Vision*, pages 618–626, 2017.
- [26] Zhiqiang Shen, Zechun Liu, Zhuang Liu, Marios Savvides, Trevor Darrell, and Eric Xing. Un-mix: Rethinking image mixtures for unsupervised visual representation learning. *arXiv preprint arXiv:2003.05438*, 2020.
- [27] Aarin van den Oord, Yazhe Li, and Oriol Vinyals. Representation learning with contrastive predictive coding. *arXiv preprint arXiv:1807.03748*, 2018.
- [28] Catherine Wah, Steve Branson, Peter Welinder, Pietro Perona, and Serge Belongie. The Caltech-UCSD Birds-200-2011 Dataset. Technical Report CNS-TR-2011-001, California Institute of Technology, 2011.
- [29] Xiu-Shen Wei, Jian-Hao Luo, Jianxin Wu, and Zhi-Hua Zhou. Selective convolutional descriptor aggregation for fine-grained image retrieval. *IEEE Transactions on Image Processing*, 26(6):2868–2881, 2017.
- [30] Xiu-Shen Wei, Chen-Lin Zhang, Jianxin Wu, Chunhua Shen, and Zhi-Hua Zhou. Unsupervised object discovery and co-localization by deep descriptor transformation. *Pattern Recognition*, 88:113–126, 2019.
- [31] Yuxin Wu, Alexander Kirillov, Francisco Massa, Wan-Yen Lo, and Ross Girshick. Detectron2. <https://github.com/facebookresearch/detectron2>, 2019.
- [32] Sangdoo Yun, Dongyoon Han, Seong Joon Oh, Sanghyuk Chun, Junsuk Choe, and Youngjoon Yoo. CutMix: Regularization strategy to train strong classifiers with localizable features. In *The IEEE International Conference on Computer Vision*, pages 6023–6032, 2019.

- [33] Chen-Lin Zhang, Yun-Hao Cao, and Jianxin Wu. Rethinking the route towards weakly supervised object localization. In *The IEEE Conference on Computer Vision and Pattern Recognition*, pages 13460–13469, 2020.
- [34] Hongyi Zhang, Moustapha Cisse, Yann N. Dauphin, and David Lopez-Paz. Mixup: Beyond empirical risk minimization. In *The International Conference on Learning Representations*, pages 1–13, 2018.
- [35] Bolei Zhou, Aditya Khosla, Agata Lapedriza, Aude Oliva, and Antonio Torralba. Learning deep features for discriminative localization. In *The IEEE Conference on Computer Vision and Pattern Recognition*, pages 2921–2929, 2016.

Table 8: Comparisons of localization accuracy (without training using SCDA) on ImageNet and CUB-200, and classification accuracy (after training) on CIFAR-10 using different initialization methods. We report the average accuracy and standard deviation of 3 trials.

Initialization method	Loc acc. (w/o training)		Clss acc. (after training)
	ImageNet	CUB-200	CIFAR-10
Kaiming normal (used in the paper)	48.2 \pm 0.6	41.8 \pm 0.6	83.4 \pm 0.3
Kaiming uniform	49.2 \pm 0.6	43.3 \pm 0.6	82.7 \pm 0.7
Xavier normal	42.2 \pm 1.1	32.6 \pm 0.9	80.9 \pm 0.6
Xavier uniform	41.3 \pm 1.0	33.3 \pm 0.6	80.4 \pm 0.4
Normal(0,0.1)	50.6 \pm 0.3	43.4 \pm 0.5	82.8 \pm 0.8
Normal(0,1)	0.0 [*]	0.0 [*]	77.4 \pm 0.8
Uniform(-0.1,0.1)	50.0 \pm 0.4	43.4 \pm 0.4	82.3 \pm 0.3
Uniform(-1,1)	0.0 [*]	0.0 [*]	79.5 \pm 0.5
Zero init	0.0 [*]	0.0 [*]	10.0 \pm 0.0

^{*} When using Normal(0,1) or Uniform(-1,1) for initialization, the network fails to localize objects (obtain nearly all zero activation map and the localization accuracy is actually 0).

A Appendix

The appendix contains more visualization results, experimental details and experimental results not included in the main paper.

A.1 Visualization and localization results

In Section 4.1 (Table 1) in the main paper, we analyzed the localization ability of randomly initialized ResNet-50 and we present more visualization results of Table 1 here. We also investigate the effect of different initialization methods.

Results of using different initialization methods. Notice that we used PyTorch default initialization method Kaiming normal initialization in the paper. Now we investigate the effect of other initialization methods, i.e., Kaiming uniform, Xavier normal, Xavier uniform, Normal(0,0.1), Normal(0,1), Uniform(-0.1,0.1), Uniform(-1,1) and zero init for experiments, and the localization results are shown in Table 8. We can observe that other initialization methods (e.g., Kaiming uniform, Normal(0,0.1) and Uniform(-0.1,0.1)) can also get good and robust localization results and Tobias is actually a general phenomenon. However, we can not expect a good localization result with inappropriate initialization methods. For instance, when we set all the weights to zero, we will get all zero activation map and zero localization accuracy (it will also destroy supervised training with this bad initialization). Also, we design an experiment to investigate the relationship between the localization accuracy of a random network before any training and its classification accuracy after training. We train on CIFAR-10 for 60 epochs using ResNet-50 with different initialization methods as aforementioned. We can observe that the localization accuracy of a random network can somehow indicate its classification accuracy after training (i.e., has high correlation). For instance, Normal(0,1) has much worse localization performance than Normal(0,0.1) (without any training using SCDA) and it also gets lower accuracy after training on CIFAR-10. Also, Xavier initialization performs worse on localization than Kaiming initialization and lower classification accuracy after training is observed. In other words, we observe that a random network that sees objects better is more likely to perform better for classification after training.

Visualization of multiple randomly initialized ResNet-50. From Table 1 we have seen that a randomly initialized results can get robust localization results and it achieves a low standard deviation of 0.6 on ImageNet and CUB-200, respectively. We show some visualization results of 3 randomly initialized ResNet-50 using SCDA on ImageNet and CUB-200 in Figure 4 and Figure 5, respectively. We color foreground regions $((i, j) | M_{i,j} = 1)$ with red. We can intuitively see that the localization results of different randomly initialized ResNet-50 are very similar and it further suggests that Tobias is one inductive bias of CNN. Also, we can observe that a randomly initialized CNN can localize objects surprisingly well, which is comparable to the ImageNet supervised counterpart.

Visualization of using different activation functions. We change the default activation function ReLU to sigmoid and arctan for a randomly initialized ResNet-50 and show the results on ImageNet in Figure 6. As can be seen, ReLU achieves significantly better localization performance than sigmoid and arctan. It demonstrates that ReLU plays an important role in modern CNNs to deactivate texture-less backgrounds and activate objects.

Visualization of ResNet-50 with different depth. We visualize the localization results of different stages for ResNet-50 in Figure 7. From Figure 7 we can see that shallow layers focus more on local edges and textures and the network can better localize the whole object as the depth of the network increases. For instance, in column (b), (d), (e), (f) and (h) in Figure 7, shallow layers (e.g., ‘conv1’ or ‘conv1-2’) will be confused of (i.e., focus on) the texture or edge of backgrounds (e.g., grass or floor) while the full network (‘conv1-5’) can successfully see the whole object. It indicates that the depth of network (i.e., the number of ReLU and max pooling layers) is crucial for a randomly initialized ResNet-50 to localize objects.

More successful and failure cases: Here we present more successful cases on ImageNet, CUB-200 and VOC 2007 in Figure 8, as a supplement to Figure 1 in the paper. Furthermore, we present some failure cases on these 3 datasets in Figure 9. Now let’s delve into these failed cases in Figure 9. For CUB-200, the random network focuses only on the head of birds in column (a), (d) and (e) while gets confused of complex backgrounds in column (b) and (g). For VOC2007, the random network does not localize all objects when there are multiple objects in column (a) (miss people), column (b) (miss the other cat), column (c) (miss people) and column (d) (miss other people).



Figure 4: Visualization of multiple *randomly initialized* ResNet-50 using SCDA on ImageNet. ‘Random 1’ represents the first trial and the same for ‘Random 2’ and ‘Random 3’. We color foreground regions $((i, j) | M_{i,j} = 1)$ with red

A.2 Training details

We present training details for self-supervised learning and downstream evaluation here.

Training details for SSL: The training details for MoCov2 and SimCLR on CUB200 for those experimental results presented in Table 2 in the main paper are shown in Table 9. We adopt several common data augmentations and compose them stochastically: (a) random scaling and cropping with a scaling factor chosen between [0.2, 1.0]; (b) random horizontal flipping with a probability of 0.5; (c) color distortion with a probability of 0.8; (d) color dropping (i.e., randomly convert images to grayscale with 20% probability for each image); (e) random gaussian blur.

Training details for downstream classification benchmarks: For ImageNet linear evaluation, we follow the same settings in [4]. For ImageNet fine-tuning, we train for 30 epochs with the learning



Figure 5: Visualization of multiple *randomly initialized* ResNet-50 using SCDA on CUB-200.



Figure 6: Ablation of activation functions for randomly initialized ResNet-50 on ImageNet.

rate initialized to 0.01, which is divided by 10 every 10 epochs. For other classification benchmarks, we train the network for 120 epochs with a batch size of 64 and a weight decay of 5e-4. The learning rate starts from 10.0 for linear evaluation and 0.01 for fine-tuning and is decreased every 40 epochs.

Table 9: Training details for MoCov2, SimCLR and BYOL on CUB200 for experiments presented in Table 2. τ denotes the temperature parameter and k denotes the size of the memory bank in MoCov2.

Method	backbone	Settings				
		bs	lr	lr schedule	τ	k
MoCov2	ResNet-18	128	0.03	cosine	0.2	4096
	ResNet-50	128	0.03	cosine	0.2	4096
SimCLR	ResNet-18	512	0.5	cosine	0.1	-
	ResNet-50	128	0.125	cosine	0.1	-

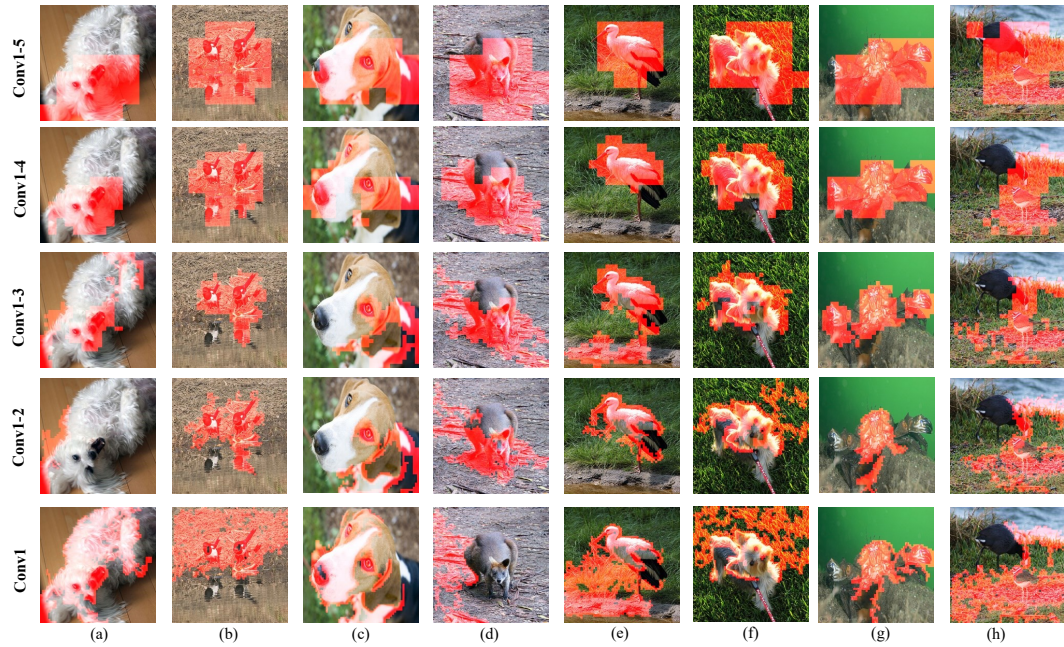


Figure 7: Ablation of network depth for randomly initialized ResNet-50 using SCDA on ImageNet.

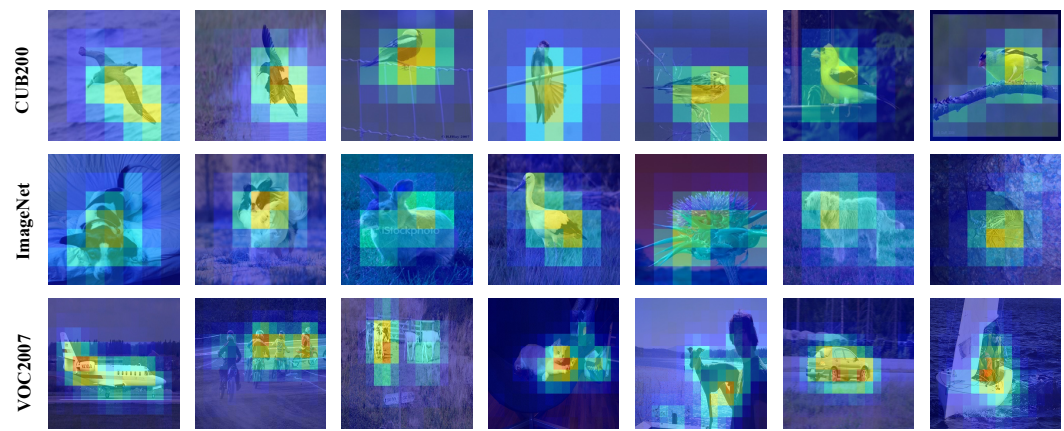


Figure 8: Visualization of localization heatmaps using SCDA for a *randomly initialized* ResNet-50. Best viewed in color when zoomed in.

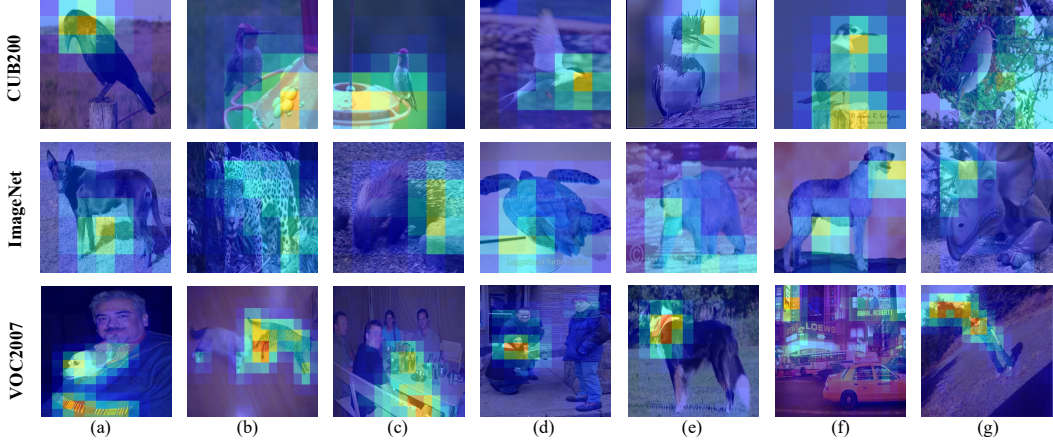


Figure 9: Visualization of some failure cases using SCDA for a *randomly initialized* ResNet-50. Best viewed in color when zoomed in.

Table 10: Downstream object detection performance on VOC 07&12 and linear evaluation accuracy on Tiny-ImageNet-200 when pretrained on ImageNet subsets using ResNet-50 (with different hyper-parameter p).

pretraining			VOC 07&12			Tiny-IN-200
method	#images	epochs	AP ₅₀	AP	AP ₇₅	
random init.	0	0	63.0	36.7	36.9	0.5
MoCov2			71.1	43.6	45.8	0.5
MoCov2-Tobias ($p=0.3$)	10,000	200	71.4 (+0.3)	44.3 (+0.7)	47.0 (+1.2)	9.9 (+9.4)
MoCov2-Tobias ($p=0.5$)			71.5 (+0.4)	44.3 (+0.7)	47.3 (+1.5)	10.2 (+9.7)
MoCov2			71.6	43.9	45.9	23.6
MoCov2-Tobias ($p=0.3$)	10,000	800	73.2 (+1.6)	45.7 (+1.8)	48.5 (+2.6)	23.9 (+0.3)
MoCov2-Tobias ($p=0.5$)			73.9 (+2.3)	46.3 (+2.4)	49.4 (+3.5)	23.3 (-0.3)
MoCov2			72.2	44.7	46.8	26.3
MoCov2-Tobias ($p=0.3$)	50,000	200	73.7 (+1.5)	46.0 (+1.3)	49.2 (+2.4)	26.0 (-0.3)
MoCov2-Tobias ($p=0.5$)			74.7 (+2.5)	47.4 (+2.7)	50.5 (+3.7)	26.3
MoCov2			77.5	49.3	53.3	37.9
MoCov2-Tobias ($p=0.3$)	50,000	800	77.9 (+0.4)	50.3 (+1.0)	54.9 (+1.6)	40.7 (+2.8)
MoCov2-Tobias ($p=0.5$)			78.4 (+0.9)	50.9 (+1.6)	55.1 (+1.8)	39.4 (+1.5)
MoCov2			76.2	48.0	51.6	35.3
MoCov2-Tobias ($p=0.3$)	100,000	200	77.5 (+1.3)	49.8 (+1.8)	53.9 (+2.3)	36.5 (+1.2)
MoCov2-Tobias ($p=0.5$)			76.8 (+0.6)	49.2 (+1.2)	53.3 (+1.7)	36.4 (+1.1)

A.3 More results

We set the hyper-parameter p to 0.3 for all experiments in the main paper and we have seen that we can get better results with more carefully tuned p in Section 4.3. Here we investigate the influence of data volume on hyper-parameter selection and present more results by setting different p values on ImageNet subsets in Table 10.

As shown in Table 10, we can get much better performance with more carefully tuned p . For instance, when both trained for 200 epochs on IN-50k (50,000 images), our Tobias (with $p=0.5$) achieves better results than those reported in the main paper (with $p=0.3$), and is significantly better than baseline counterpart: up to **+2.5** AP₅₀, **+2.7** AP and **+3.7** AP₇₅. It confirms that our method has the potential to perform better with more carefully tuned p . Also, we can observe that when trained for 200 epochs on IN-100k, $p=0.5$ achieves worse results than $p=0.3$, which indicates that A higher p value is more suitable for small data while a lower p value is more suitable for large data.